Journal of Advanced Research 55 (2024) 89–102

Contents lists available at ScienceDirect

Journal of Advanced Research

journal homepage: www.elsevier.com/locate/jare

Original Article

Duo-role Platelet-rich Plasma: temperature-induced fibrin gel and growth factors' reservoir for microneedles to promote hair regrowth

Yang Sun [a,b], Lunan Yang [a], Lijuan Du [a], Yi Zhou [a], Kaige Xu [b], Jian Chen [a], Ye He [a], Qian Qu [a], Yong Miao [a,*], Malcolm Xing [b,*], Zhiqi Hu [a,*]

[a] Department of Plastic and Aesthetic Surgery, Nanfang Hospital, Southern Medical University, Guangzhou, Guangdong 510515, China
[b] Department of Mechanical Engineering, University of Manitoba, 75A Chancellors Circle, Winnipeg, Manitoba R3T 2N2, Canada

HIGHLIGHTS

- A temperature-sensitive Platelet-rich Plasma (PRP) induced fibrin gel interpenetrated with the GelMA on a detachable transdermal microneedle (MN) for hair regrowth.
- Duo-role PRP: temperature-induced fibrin gel as microneedle's enhanced network and GFs reservoir for microneedles to promote hair regrowth.
- PRP-released GFs can be anchored into a GelMA/PRP matrix with an increased lifespan for a truly controlled release.
- The application of PRP-MNs has promising effects and more cost-effective for hair regrowth due to the synergistic effect of multiple GFs.
- PRP-MNs can benefit many other applications, such as oral and maxillofacial surgery, refractory wound, skin disease and rejuvenation, and reproductive medicine.

GRAPHICAL ABSTRACT

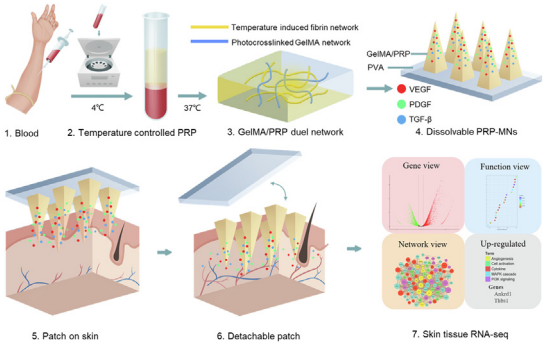

ARTICLE INFO

Article history:
Received 19 October 2022
Revised 20 February 2023
Accepted 22 February 2023
Available online 26 February 2023

Keywords:
Hair regrowth microneedle patch
platelet-rich plasma (PRP) induced fibrin network
Thermal sensitive PRP gel
Fibrin penetrated GelMA microneedle

ABSTRACT

Introduction: Alopecia concerns more than half our adult population. Platelet-rich plasma (PRP) has been applied in skin rejuvenation and hair loss treatment. However, the pain and bleeding during injection and the troublesome for fresh preparation of each action limit PRP's in-depth applying dedication to clinics.
Objectives: We report a temperature-sensitive PRP induced fibrin gel included in a detachable transdermal microneedle (MN) for hair growth.
Results: PRP gel interpenetrated with the photocrosslinkable gelatin methacryloyl (GelMA) to realize sustained release of growth factors (GFs) and led to 14% growth in mechanical strength of a single microneedle whose strength reached 1.21 N which is sufficient to penetrate the stratum corneum. PRP-MNs' release of VEGF, PDGF, and TGF-β were characterized and quantitatively around the hair follicles (HFs) for 4–6 days consecutively. PRP-MNs promoted hair regrowth in mice models. From transcriptome

* Corresponding authors.
E-mail addresses: miaoyong123@i.smu.edu.cn (Y. Miao), malcolm.xing@umanitoba.ca (M. Xing), huzhiqidr163@i.smu.edu.cn (Z. Hu).

https://doi.org/10.1016/j.jare.2023.02.014

Growth factor reservoir

sequencing, PRP-MNs induced hair regrowth through angiogenesis and proliferation. The mechanical and TGF-β sensitive gene Ankrd1 was significantly upregulated by PRP-MNs treatment.
Conclusion: PRP-MNs show convenient, minimally invasive, painless, inexpensive manufacture, storable and sustained effects in boosting hair regeneration.

Introduction

Alopecia is becoming a worldwide concern for the public, which is a hair disorder marked by the progressive miniaturization of hair follicles (HFs) and a shortening anagen phase, resulting in a reduction in scalp hairs [1]. Although alopecia does not affect physical health, it negatively affects the social and psychological well-being of patients, causing reduced quality of life. Early diagnosis and treatment can significantly delay the progression of alopecia and improve prognosis. Treatments include pharmaceuticals, such as Minoxidil and Finasteride, which require long-term patient compliance with varying effectiveness [2,3]. Common side effects include sexual dysfunction, depressive alteration of mood, and skin irritation [4,5]. Surgical effectiveness is influenced by the surgeon's proficiency and is only suitable for patients with sufficient donor hairs [6,7]. Additionally, unnatural hairline and donor area scars are frequently reported concerns [8].

Platelet-rich plasma (PRP) is a platelet concentrate extracted from autologous blood. The clinical efficacy of PRP depends mainly on the concentration of platelets and their growth factors (GFs) (VEGF, PDGF, TGF-β, etc.), especially during the healing process, where they are responsible for the proliferation, differentiation, chemotaxis, and tissue morphogenesis [9]. Once activated, multiples types of GFs are released from PRP, which can promote telogen HFs to re-enter the hair cycle, PRP has gradually become an effective and promising option for hair loss treatment [10–12]. In bedside, PRP is injected into the scalp through a hypodermic needle (30-32G) [10]. However, it is painful and causes bleeding. Besides, it must be freshly prepared for usage. PRP needs to be applied under the operation of physicians after giving patients surface anesthesia. These concern the clinical application of PRP.

MNs are micron-scale needles used for drug delivery, with a length between 500 and 1000 μm. MNs are developing rapidly as non-invasive transdermal drug delivery, vaccination, patient monitoring, and disease diagnosis [13,14], with the advantages of being painless, minimally invasive, and easy to operate. In addition, the application of MNs does not result in the loss of PRP by diffusion in the deep dermis caused by uneven control of the syringe depth. MNs can be effectively confined to the superficial dermis, achieving a high concentration of PRP sustained release around the HFs.

Recently, researchers have started to focus on MNs for hair regrowth by achieving local delivery of exosomes [15], valproic acid [16], finasteride [17], or nanozyme [18], avoiding the side effects associated with the systemic application of drugs. Although these MNs strategies have achieved some therapeutic effects, MN matrices closely matched with the microenvironment of HF for comprehensive regulation of hair regrowth and with the lowest cost need to be developed. PRP is autologous in origin and easy to obtain. More essentially, GFs can meet the comprehensive regulation of hair regrowth. However, PRP has not been reported about the hair application in combination with MNs due to its limitations of liquid form and difficult storage.

In our study, we developed a temperature-sensitive PRP induced fibrin gel as MN's enhanced network and GF reservoir which was then interpenetrated with the photocrosslinkable gelatin methacryloyl (GelMA) on a detachable transdermal MN for hair regrowth. (Scheme 1). Gelatin is a natural hydrogel close to the dermis composition where the HFs are located [19]. After applied to the skin and the base detached, the MNs can be targeted to reach the HFs bulge area and hair bulb where 2 kinds of HFs stem cells are located. HF bulge stem cells determine the proliferation and lineage differentiation of HF epidermal components [20]. The DP determines the size of HFs and the transition of the hair cycle [21]. We also explored the PRP temperature-sensitive characteristic to produce the gelation of the fibrin network and quantify the released GFs. With these attributes, PRP-released GFs can be anchored into a GelMA/PRP-induced fibrin matrix with an increased lifespan for a truly controlled release [22]. To advance our understanding of PRP-MNs, transcriptome sequencing was conducted and revealed that the PRP-MNs induced hair regrowth through angiogenesis and proliferation. The mechanical and TGF-β sensitive gene Ankrd1 was studied.

Results

Fabrication and characterization of temperature-controlled PRP and GelMA

A temperature-controlled PRP was prepared under a cryogenic environment (4℃). Red blood cell (RBC), platelet (PLT), and white blood cell (WBC) concentrations of the whole blood and PRP groups were summarized in Table 1. Hematology analysis showed that the majority of RBC and WBC were removed by PRP procedure, while the platelet distribution peak and width remained unchanged (Fig. 1**A**). However, PRP becomes fragile and loses biological activity after leaving the physiological environment. Thus, PRP lyophilization for preserving stable PRP effect and increasing concentration was utilized. To verify the GFs concentration of PRP lyophilization, we set 2 groups for ELISA protein quantification: (i)activated-PRP (a-PRP, the activated platelets in PRP release multiple GFs) was obtained by incubating PRP at 37 ℃ for 15 mins, (ii) freeze-dried product from inactivated PRP (FD-PRP, PRP remained inactivated under 4℃) (Fig. 1**B).** PRP contains mainly platelet-derived GFs, including VEGF, PDGF, TGF-β1, IGF-1, and EGF [9,23]. In particular, PDGF is the most predominant in PRP and plays a crucial role in the development of dermal papilla for hair regrowth [10,24]. TGF-β1 induces the anagen phase of the hair cycle and regulates angiogenesis [25]. Additionally, VEGF promotes angiogenesis, an essential factor in hair regrowth [26]. PDGF-BB, VEGFA, and TGF-β1 were detected by ELISA in 2 groups (Fig. 1**C**). Interestingly, FD-PRP was able to release more GFs than a-PRP, which showed a significantly higher concentration of 8683 ± 591 pg/ml in PDGF-BB. This finding confirmed that PRP lyophilization can retain GFs stably and efficiently for our follow-up experiments.

Thermal and photocrosslink induced GelMA/PRP formation

A PRP-induced fibrin gel can be obtained by activating platelets to convert fibrinogen into a fibrin network under 37℃. Because of the thermal-sensitive PRP activation characteristic, we find that PRP gel had the following advantages, (i) the temperature-controlled characteristic allows us to manipulate MN shaping and GF release through thermal inducement; (ii) the autologous

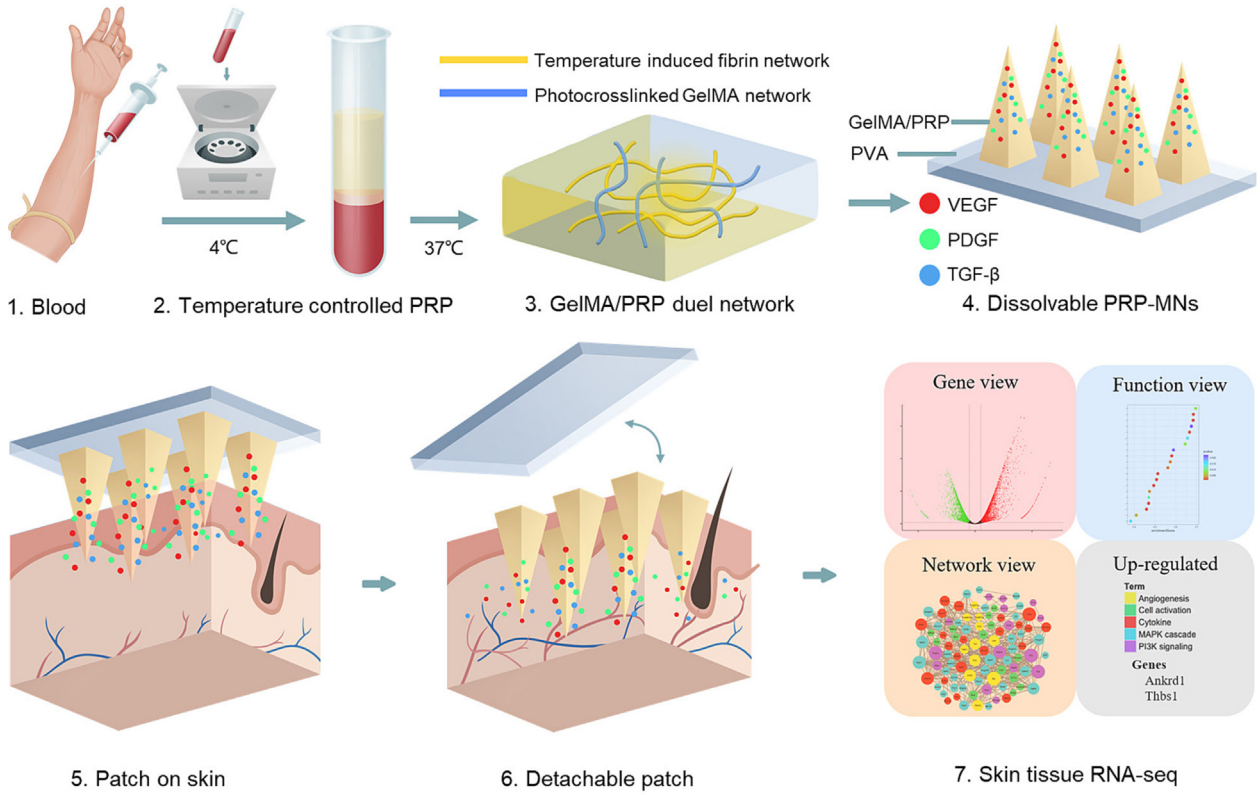

Scheme 1. A temperature-controlled PRP induced fibrin gel interpenetrated with the photocrosslinked GelMA as sustained PRP therapy for hair regrowth through a base-detachable MN system.

Table 1
Blood cell count of whole blood and PRP.

	PLT(*10^6/mL)	RBC(*10^6/mL)	WBC(*10^6/mL)
Whole blood	218.7 ± 53.1	5273.3 ± 193.6	4.2 ± 0.3
PRP	1182.7 ± 170.8	23.3 ± 12.5	0.4 ± 0.2

PRP fibrin scaffold is highly biocompatible and has a great potential for vascularizing.

Gelatin was modified by methacrylic anhydride, as shown in Fig. 1**D**, which enables it to be photocrosslinked by the photoinitiator (LAP). FTIR and ^{1}H-NMR analyses were performed to characterize synthesized GelMA. The FTIR showed the peaks at 1450 cm^{-1}(amide III), 1547 cm^{-1} (amide II), 1645 cm^{-1} (amide I), and 3308 cm^{-1} (hydroxyl group) as in Fig. 1**E**. Amides (I to III) corresponded respectively to the C = O bond vibrations, the bending of the N–H bonds, and the C-N and N–H plane vibrations [27]. The GelMA had been synthesized successfully according to these results. ^{1}H NMR was used to verify the methacrylation of gelatin. The ^{1}H-NMR spectrum of GelMA (Fig. 1**F**, red curve) showed 2 new signals at 5.4 ppm and 5.6 ppm (area a) that were attributed to the methacrylamide groups [28]. Another new signal appeared near 1.8 ppm (area c), which belonged to a function of methyl methacrylate grafting on the structure of gelatin. These indicated that methacrylic anhydride was grafted successfully. The graft ratio of ε-amino groups of gelatin was defined as the degree of methacrylation(DM). The lysine methylene signal (2.9 ppm, area b) was integrated to obtain the areas of GelMA and gelatin [29]. The DM of the GelMA could be calculated as the previous report [28], showing that the synthesized GelMA reached a high DM about 73%.

TNBS assay was used to determine the free amino groups, which can quantify DM as well. Non-modified gelatin was determined to be 0.321 ± 0.024 (mmol/g), consistent with the previous report [30]. GelMA remained 29.4% unreacted free amino groups compared to gelatin, which could quantify DM as 70.6%. The results of both methods showed that GelMA with efficient DM can be a suitable matrix for microneedle fabrication.

Fig. 1**G** showed the two-step fabrication of the GelMA/PRP-induced fibrin matrix. Briefly, GelMA and PRP were mixed first, then PRP was induced to form the first fibrin network through thermally controlled self-assembly at 37℃. GelMA was finally photocrosslinked to make the second network. PRP turned to a gel state after thermal induced fibrin network formation(Fig. 1**H**). The scanning electron microscope (SEM) images showed the microstructures of the PRP, GelMA, and GelMA/PRP hydrogels had interconnected porous microstructures (Fig. 1**I**). The PRP-induced fibrin gel was only constituted by a loosely distributed network, while the GelMA/PRP matrix was constituted by thick and uniformly packed dual networks. In conclusion, these results confirmed the successful formation of the GelMA/PRP matrix.

Fabrication and characterization of the PRP-MNs system

A four-step filling process was applied to form the detachable PRP-MNs (Fig. 2**A**). Briefly, Microneedle molds were prepared in a 10 × 10 array with 900 μm in height using PDMS. GelMA/PRP matrix containing photoinitiator (LAP) was first casted into the needle cavities under 37℃ to form a fibrin network and dry. After the concentrated matrix was photocrosslinked, the base was covered with PVA to form a detachable patch. The desiccated PRP-MNs patch was shown in Fig. 2**B, C**, in which GelMA/PRP matrix as yellow parts were observed in each tip. SEM (Fig. 2**D**) demonstrated that each microneedle has an intact and uniform morphology. It provided a pyramidal shape with a sharp tip and a base diameter of 400 μm. GelMA-MNs were fabricated to be the

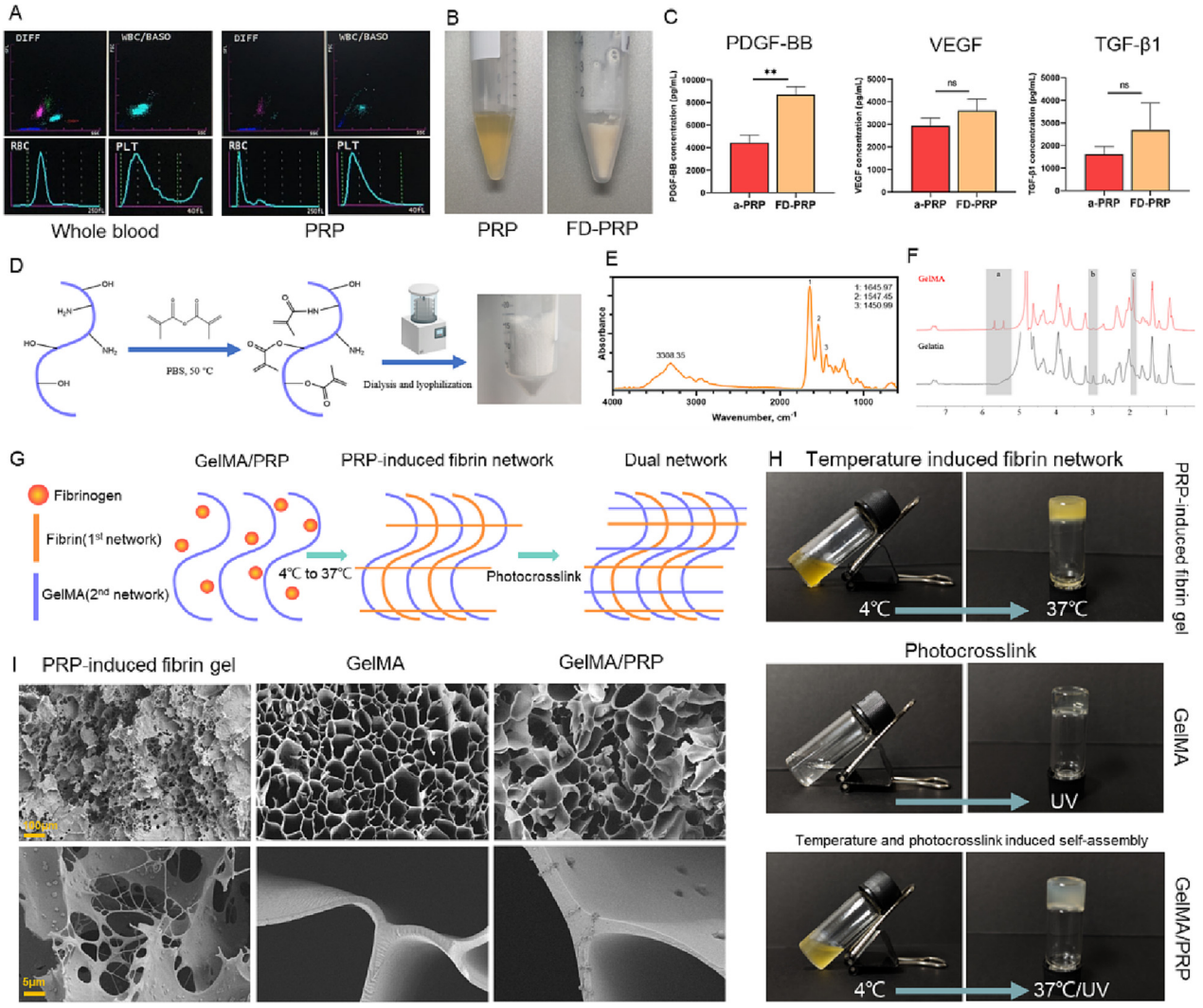

Fig. 1. Fabrication and characterization of PRP, thermal sensitive PRP-induced fibrin, and penetrated GelMA. (A) Hematology analysis showed the difference between whole blood (left) and PRP (right). (B) Photographs showed the PRP and FD-PRP products. (C) ELISA protein quantification of GFs of a-PRP and FD-PRP groups (TGF-β1, PDGF-BB, and VEGF) (n = 3). ** P < 0.01, ns = no significance. (D) Illustration of GelMA synthesis. (E) FTIR spectra of GelMA showed characteristic peaks. (F) ^{1}H-NMR spectra of gelatin and GelMA demonstrated different signal areas. (G) Illustration of the GelMA/PRP formation composed of the dual network. (H) Macroscopic observation of temperature and photocrosslink-induced GelMA/PRP formation. (I) SEM images of PRP-induced fibrin gel, GelMA, GelMA/PRP.

comparison, without filling of PRP. To confirm its ability to break through the stratum corneum barrier, the mechanical properties of PRP-MNs from different ration of GelMA/PRP (1:1; 1:2; 1:3) and simple GelMA-MNs were measured by stress–strain gauge under dynamic force (Fig. 2**E**). As shown in Fig. 2**F, S1**, the pressure versus displacement map demonstrated that PRP-MNs with a ratio of GelMA/PRP = 1:2 showed highest breaking force of 1.21 N per microneedle, since the induced fibrin network in PRP enhanced this [31]. The PRP-MNs exhibited sufficient stiffness for skin insertion(>0.17 N per microneedle) [32].

To obtain an optimal release and dissolution, we performed in vitro characterization experiments of PRP-MNs (Fig. 2**G**). PRP-MNs from three different donors were tested for dissolution ability and showed no significant difference (**Fig.S2**). Furthermore, the blend of GelMA and PRP in different proportions accelerated the dissolution of PRP-MNs. The GelMA/PRP = 1:3 group displayed the fastest dissolution, the GelMA/PRP = 1:1 group degraded slowly, and the GelMA/PRP = 1:2 group could achieve sustained release over 4 days. The PVA base dissolved rapidly within tens of minutes in PBS solution at 37℃. In the next 6 days, the GelMA/PRP matrix gradually degraded and released GFs (Fig. 2**H**). As noted, GelMA/PRP = 1:2 group could achieve sustained release over 4 days and was selected as the optimal MNs formulation accordingly. In addition, 3 GFs from the PRP-MNs were measured by ELISA. As shown in Fig. 2**I-K**, PRP-MNs released GFs rapidly from the interconnected porous microstructures to reach an effective concentration in 24 h. The GFs gradually released during PRP-MNs' degradation after 4–6 days. The ion-interaction allows basic GFs(such as TGF-β1 [33], VEGF [34], and PDGF [35]) that carried positive charges to be immobilized in GelMA, which carried negative charges in the GelMA backbone under physiological pH [36,37] (Fig. 2**L, M**). Besides, with the attribute of fibrin network, GFs could be further anchored for a truly controlled release [22]. The results showed that the PRP-MNs system achieved sustained and controlled release profiles of GFs.

To test the mechanical properties of the PRP-MNs for a suitable in vivo application, we inserted PRP-MNs into the skin of mice and removed the base after 1–2 h (Fig. 3**A**). A 10x10 array of micropores were noted at the administration site without any other skin damage. The micropores gradually became invisible within 1 h and completely disappeared within 24 h after base removal. As shown in Fig. 3**B**, the needles rehydrated and separated from the PVA base

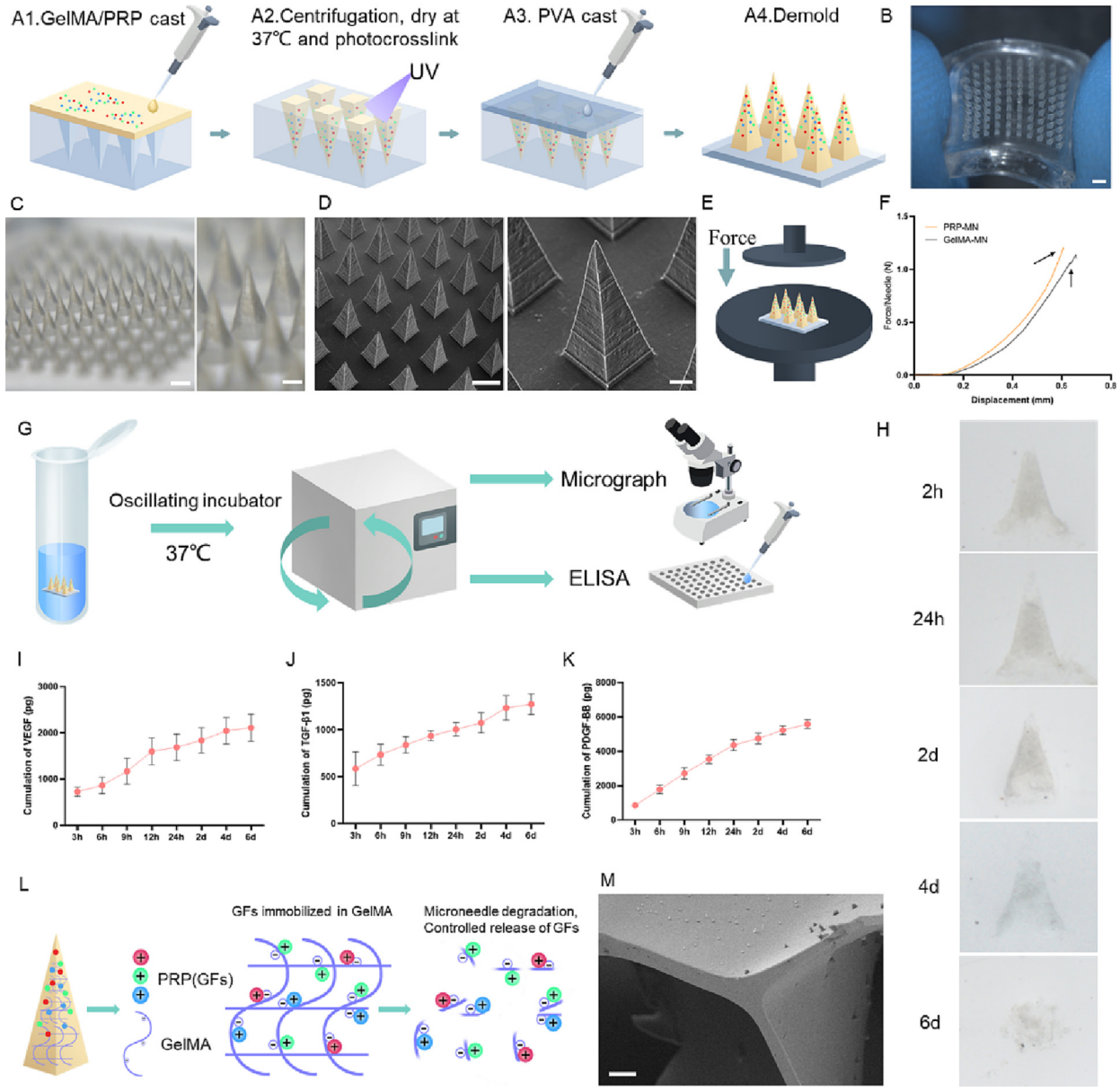

Fig. 2. Fabrication and in vitro characterization of PRP-MNs system. (A1-4) Schematic representation of the fabrication process of PRP-MNs. (B) Digital photograph of PRP-MNs. Scale bar, 1 mm. (C) Microscopic photograph of PRP-MNs. Scale bar, 500 μm (left), 200 μm (right). (D) SEM image of PRP-MNs. Scale bar, 500 μm (left), 100 μm (right). (E) Schematic representation of compressive test. (F) The force (per microneedle) versus displacement of the patch. The sudden drop was considered as the breaking force of the MNs (arrows). (G) Schematic representation of in vitro characterization of PRP-MNs. (H) In vitro microneedle degradation test. Microscopic photographs of dissolvable MNs in PBS at various times. In vitro cumulative release of VEGF (I), TGF-β1(J), and PDGF-BB (K) from the PRP-MNs patch at various times. Orange points represent mean ± SD (n = 3). Error bars indicate SD. (L) Schematic representation of sustained release of PRP-MNs. The GFs from PRP are immobilized in the crosslinked GelMA through ionic and physiochemical interaction. (M) SEM image showed GFs immobilized in GelMA/PRP. Scale bar, 5 μm. (For interpretation of the references to color in this figure legend, the reader is referred to the web version of this article.)

after removal. H&E staining revealed that the microneedle remained in the skin, locating on the place where the HF stem cells were (Fig. 3**C**). The skin post-administration of PRP-MNs showed fast resealing without any erythema, which can prevent the infection of pathogenic microbes. At the same time, PRP-MNs can stay in the hair area and release GFs sustainably.

For tracing the release and degradation of the PRP-MNs system in vivo, we added Rhodamine B as a tracer to make RB-MNs (Fig. 3**D, E**). The successful insertion was further confirmed using RB-MNs, as shown in Figure Fig. 3**F**, where the skin of mice with puncture sites was stained with the released dye. After removal of the patch, RB-MNs resulted in an even distribution of the dye in a 10X10 array, suggesting that the MNs system was able to release in the skin (Fig. 3**G, H**). Over time, the color faded over 24 h as the tracer dye diffused into the skin. In vivo fluorescent imaging of mice treated with RB-MNs showed sustained fluorescence signal within 4–6 days (Fig. 3**I**). At 2d after administration, the fluorescence intensity decreased by>60% compared to 0d. This should be due to the sustained release of dye from the porous microstructures of the GelMA/PRP matrix.

PRP-MNs induce hair regrowth in vivo.

Fig. 4**A** showed representative photographs of the hair regrowth process using the 8-week-old shaved C57BL/6J mice model. The study was performed by PRP-MNs, MNs (GelMA-MNs), PRP subcutaneous injection, and the untreated group (NC). Both PRP-MNs and PRP groups used the same dose of PRP. Fig. 4**B** illustrated

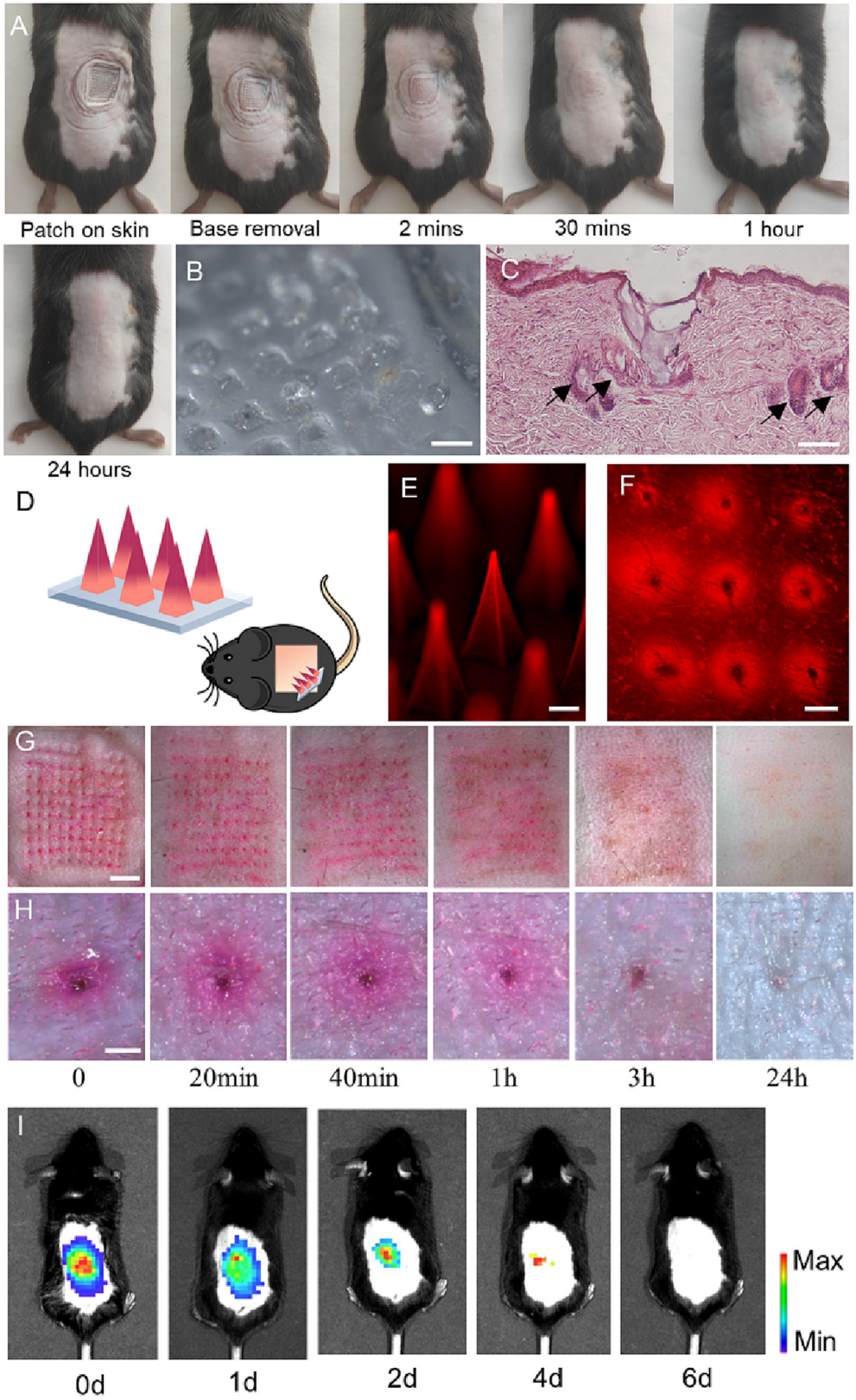

Fig. 3. In vivo penetration and release profile of PRP-MNs system. (A)Photographs of mouse applied with PRP-MNs and various times after removal. (B)Microscopic photograph of PRP-MNs base after applied on the skin. Scale bar, 500 μm. (C) H&E staining image of the skin with PRP-MN inside and base removal. PRP-MN reached the hair bulb (arrows). Scale bar, 200 μm. (D) Scheme of RB-MNs for in vivo release experiment. (E) Fluorescent photograph of RB-MNs. Scale bar, 200 μm. (F) Horizontal fluorescent photographs of the skin showed successful penetration and diffusion of the RB-MNs. Scale bar, 500 μm. (G) In vivo dissolution and diffusion profile of the RB-MNs. Scale bar, 2 mm. (H) Magnified view of a single pore. Scale bar, 500 μm. (I) In vivo fluorescent imaging of dorsal skin treated with RB-MNs.

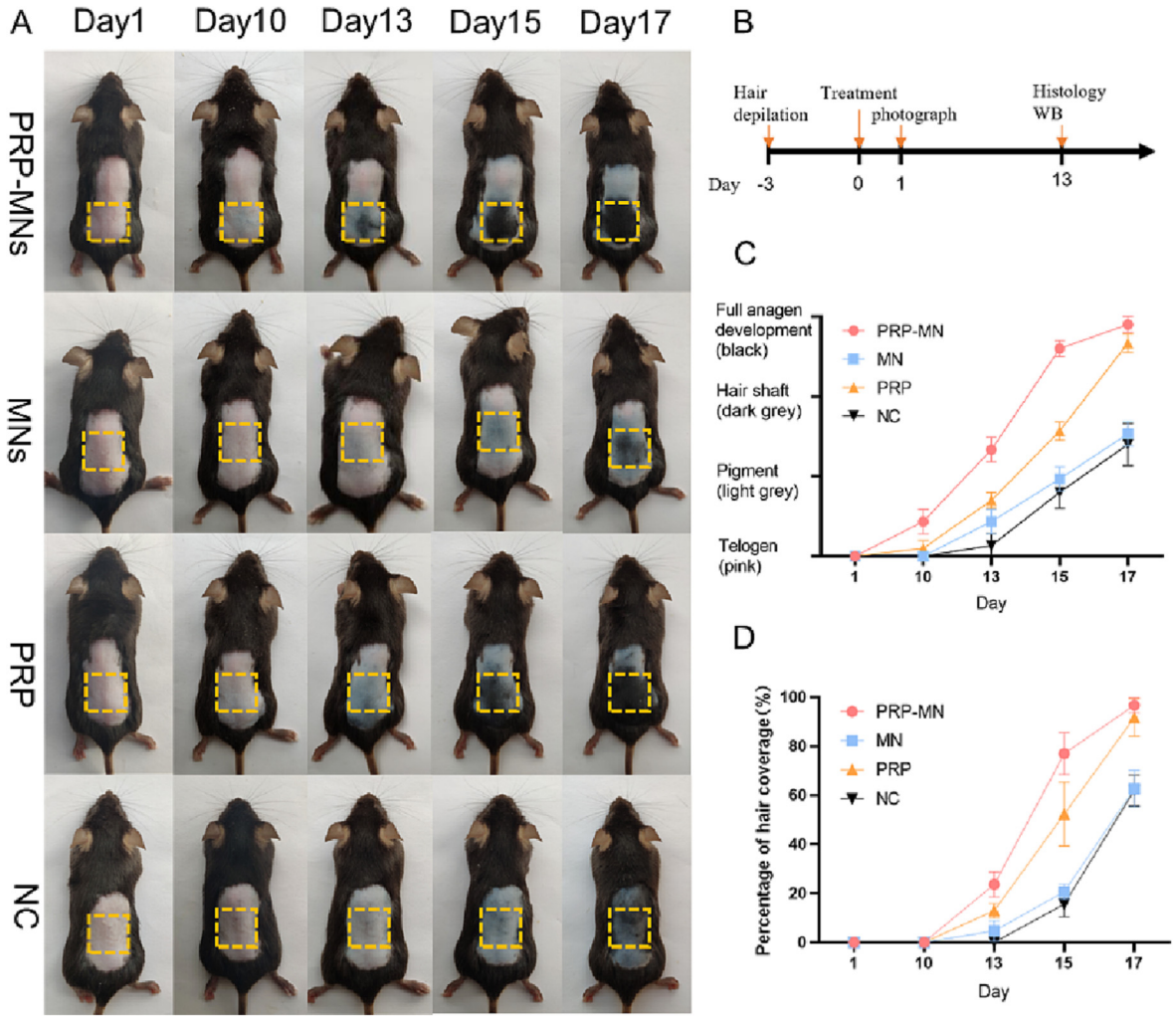

Fig. 4. PRP-MNs induce hair regrowth in vivo. (A) The treated dorsal skin was photographed at 1, 10, 13, 15, and 17 days after the administration of PRP-MNs. (B) Schematic representation of the animal experiments. (C) Hair phenotype transformed over time. (D) Percentage of hair coverage in the treated area.

the design. In contrast to the other groups after 13 days, earlier hair regrowth was initiated by PRP-MNs in the area of application. Hair shafts were already observed approximately in 30% of the treated area, while no hair shaft was found outside the treated area. As shown in the time profile of the hair phenotype transformation (Fig. 4**C**), subcutaneous PRP injections produced poorer efficacy compared to the PRP-MNs, with the treated area just starting to pigment after 13 days. Mice without any treatment or treated with blank MNs showed no significant hair regrowth at 13 days, indicating that the hair follicles were still in the telogen or early anagen phase of the hair cycle [38,39]. However, the MNs group showed earlier pigment on the treated area compared to the NC group, suggesting an effect of MNs on the initiation of the anagen phase. Hair coverage measurements showed that PRP-MNs exhibited 77% hair regrowth after 15 days (Fig. 4**D**). In contrast, the PRP group resulted in only 52.3% hair regrowth, while the others had only 20.6% and 15.6%. Together, the results showed that PRP-MNs were the most efficient in promoting the hair cycle anagen phase transformation.

Histological analysis further confirmed that PRP-MNs promoted hair regrowth using HE staining of dorsal skin after 13 days (Fig. 5**A**). Skins treated with PRP-MNs exhibited typical characteristics of mid-late anagen, such as thickened dermis and enlarged hair bulb extending into subcutis. Mice skin treated with PRP-MNs and MNs showed no obvious damage on day 13 (Fig. 5**B**), implying the high biocompatibility of the PRP-MNs system. By contrasting Fig. 3**C** with Fig. 5**B**, it revealed that the epidermal change induced by the PRP-MNs was reversible and that the normal epidermal properties were not damaged. In addition, negligible inflammation cells were found in the treated skin area by HE-staining. The difference in hair density and morphology could be clearly seen at the boundary between PRP-MNs treated, MNs treated, and untreated skin (Fig. 5**B**). The quantification analysis of the hair density was the densest in the PRP-MNs group (761.4 ± 64.78 hairs/cm^2), which had significant differences with other groups (Fig. 5**C**). Evidenced by the proportion of distinct hair cycle stages, PRP-MNs achieved the most effective promotion of the anagen phase (Fig. 5**D**). Interestingly, MNs group also showed its potential to promote hair regrowth both in density and morphology. These results implied that PRP-MNs obtained the fastest induction of hair regrowth, without irreversible skin damage.

Western-blot analysis exhibited that the protein expression level of PCNA, VEGFA, and β-catenin strongly increased after treatment with PRP-MNs, PRP, and MNs (Fig. 5**E**). These proteins were associated with proliferation, angiogenesis, and hair cycle activation [26,40,41].

PRP-MNs promote hair regrowth and angiogenesis via Ankrd1 activation

Furthermore, we assessed hair regrowth by immunofluorescence of Ki67, CD31, and β-catenin (Fig. 6**A**). Ki67 was mostly expressed in proliferating hair matrix cells [42]. PRP-MNs group

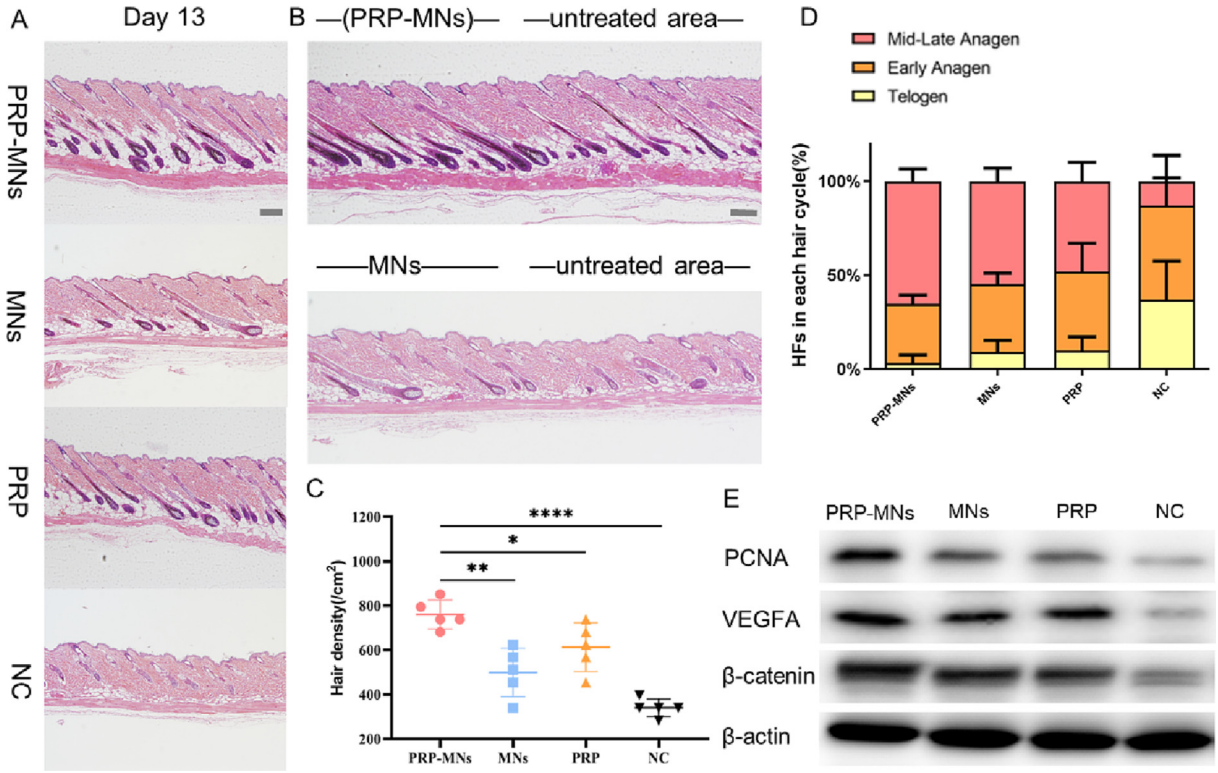

Fig. 5. Hair regrowth evaluation. (A) HE-stained sections of dorsal skin from the PRP-MNs group after 13 days exhibited more mature and denser HFs than other groups. Scale bar, 50 μm. (B) Overall view sections from treated area to the outside. Scale bar, 50 μm. (C) Hair density was significantly higher in PRP-MNs than in other groups. Each bar represents the mean ± SD (n = 5). *P < 0.05, ** P < 0.01, ****P < 0.0001. (D) Percentage of hair follicles in each phase. PRP-MNs had the highest proportion of mid-late anagen hairs and the lowest proportion of telogen hairs. Each bar represents the mean ± SD (n = 5). (E) Western-blot analysis revealed that PRP-MNs induced peak expression of PCNA, VEGFA, and β-catenin.

expressed significantly more Ki67 positive cells than PRP and NC groups (Fig. 6**B**). Vessel density revealed that PRP-MNs promoted angiogenesis most during hair regrowth, assessed by CD31 (Fig. 6**C**) [26]. Also, β-catenin staining showed that PRP-MNs most induced hair morphogenesis (Fig. 6**D**) [41]. These data indicated that PRP-MNs promoted hair regrowth and telogen-anagen transition.

To fully investigate the molecular changes caused by the application of PRP-MNs to mouse skin at an early stage (24 h), RNA was collected for transcriptome sequencing following treatment of four groups (PRP-MNs, MNs, PRP, NC; each group was pooled from three replicates at the same condition). The analysis revealed that the PRP-MNs group underwent significant upregulation of multiple regulatory genes compared to the NC group (Fig. 7**A**). Although a large proportion of the differentially expressed genes (DEGs) were the same, there were more DEGs in the PRP-MNs versus NC groups compared to the MNs and NC groups (Fig. 7**B**). According to gene set enrichment analysis (GSEA), the biological process of gene ontology (GO) enrichment differed significantly between PRP-MNs and NC groups (Fig. 7**C**). The application of PRP-MNs significantly upregulated the transcription of genes associated with angiogenesis, cytokine stimulation, cell activation, proliferative signaling, and protein metabolism. In addition, the MNs group has significant upregulation of genes related to angiogenesis, proliferative signaling, trauma stimulation, organ regeneration, and extracellular matrix remodeling. In agreement with our previous experiments, this indicated that PRP-MNs activated GFs, angiogenesis, and hair proliferation-related signals.

Based on the above function categories, screening for relevant DEGs further selected 96 genes with significant changes. We noticed that angiogenesis and proliferative signaling related genes were upregulated in the PRP-MNs, MNs, and PRP groups compared to the NC group (Fig. 7**D**), with PRP-MNs expression being the highest, which was consistent with our previous hair regrowth experiments. To confirm whether these altered genes interact with each other, we processed the protein-protein interaction (PPI) network with the STRING database (Fig. 7**E**). A strong correlation was found between the function of angiogenesis (Ret, Thbs1, Tnf), GFs stimulus (Ankrd1, Itga4), and PI3K signaling (Ptpn6) in PRP-MNs versus NC. To further validate key regulators in response to GFs stimulus (Ankrd1, Thbs1) and MAPK cascade (Itgb1), RT-PCR was performed among four groups (Fig. 7**F**), which demonstrated better hair regrowth microenvironment after PRP-MNs application. Among them, Ankrd1 was significantly upregulated and reported as a mechanical and TGF-β sensitive gene in previous studies [43]. All these data suggest that PRP-MNs promote angiogenesis and hair proliferation at the transcriptome level.

Discussion

The platelets in PRP can release multiple GFs [9,44], binding to HF stem cells in the bulge area, which is responsible for hair cycle regulation and hair differentiation, thus activating the hair into the anagen phase [23,45]. Also, GFs promote the proliferation of dermal papilla cells; elevate the expression of β-catenin, prolonging the anagen phase and delaying its transition to the catagen phase [46]. To date, some clinical trials include PRP, HF stem cells, and adipose-derived mesenchymal stem cells (AD-MSCs) injections have shown that autologous regenerative treatments can promote hair regrowth in alopecia patients, making them the novel and effective treatment options for hair loss [47–50]. However, it was reported that the bioactivity of GFs in platelets was maintained for only 6 h when PRP was prepared under conventional conditions, after which it decreased in a time-dependent manner [51].

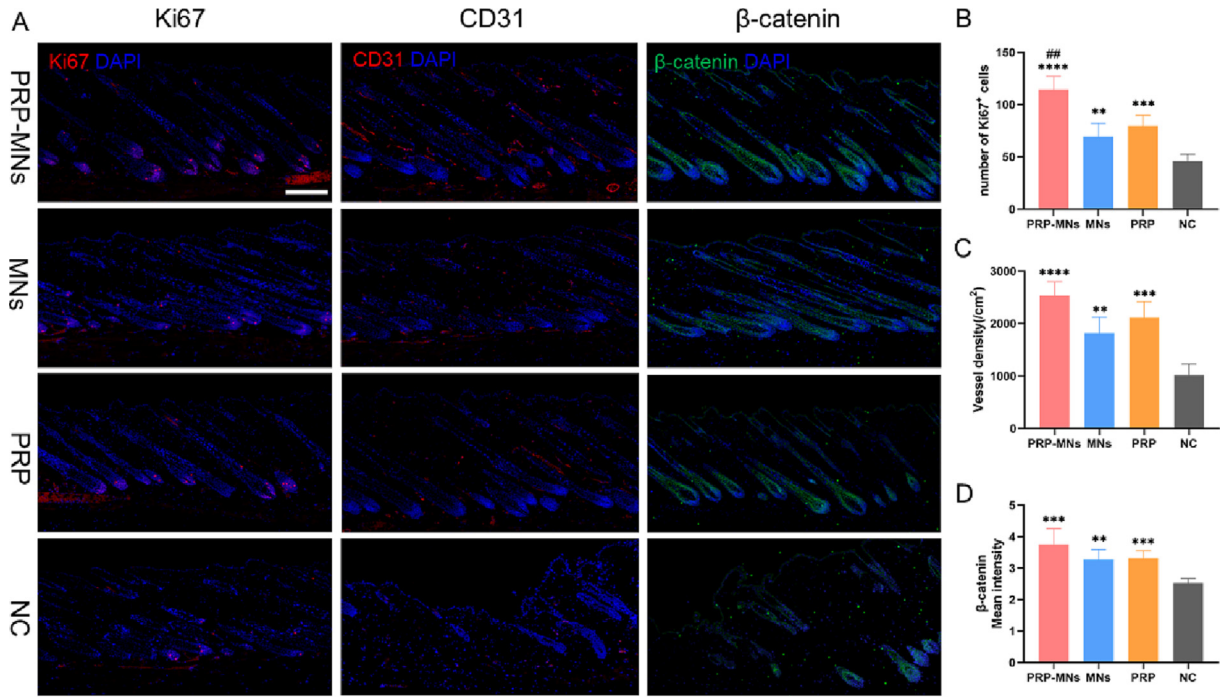

Fig. 6. PRP-MNs upregulated protein expression of hair regrowth. (A) Immunofluorescence images of Ki67, CD31, and β-catenin after 13 days. Scale bar, 200 μm. (B) PRP-MNs group expressed the highest Ki67 protein after 13 days. Ki67 expression was higher in MNs or PRP than in the NC group, and there was no difference between the MNs and PRP groups. (C) Vessel density was significantly higher in PRP-MNs, MNs, or PRP than in the NC group, whereas there was no difference between the PRP-MNs and PRP groups. (D) PRP-MNs significantly increased β-catenin expression. Each bar represents the mean ± S.D (n = 5). **, $p < 0.01$, ***$P < 0.001$, ****$P < 0.0001$ relative to the NC group; ##, $p < 0.01$ relative to PRP group.

Despite recent advances in the field, complications and side effects of PRP application still need to be overcome, including headaches, erythema, drowsiness, mild pain, scalp sensitivity, and temporary swelling [52,53].

Recent studies confirmed that hair regrowth required vascularization support [26] and that reduced HF angiogenesis was associated with some types of hair loss [54–56]. Most previous studies used only single pro-angiogenic GF, and some studies used plural pro-angiogenic GFs in concert [26,57,58]. Based on the bionic principle, the study characterized that angiogenesis was precisely regulated by different GFs at different stages, and therefore the synergistic effect of multiple GFs was more favorable for vascularization [59]. However, the combined use of multiple recombinant GFs makes the experiment complex and costly until the PRP solved this challenge. PRP derives from patients' own blood and contains a group of pro-angiogenic GFs in physiological proportions, which is more cost-effective. Recent studies characterized that PRP had promising effects on HF vascularization [60,61]. Here we found that mice showed significantly higher hair regrowth efficiency and vascularization density after the application of PRP-MNs. The expression of angiogenesis-related genes was upregulated significantly in the PRP-MNs group compared to other groups, which was consistent with the results of histological experiments.

Here we developed a temperature-sensitive PRP induced fibrin gel interpenetrated with the GelMA on a detachable transdermal MN to provide enhanced network and GF reservoir. Based on the fact that the natural PRP fibrin scaffold has a great potential for vascularizing [62] and GelMA is close to the dermal composition, making it highly biocompatible, functional, and degradable for hair microenvironment [81–83]. The temperature-controlled characteristic allows us to manipulate MN fabrication and GF release through thermal inducement. Besides, the GelMA/PRP anchored the GFs' release in a controlled way with interconnected porous microstructures from dual network. It was worth mentioning that PRP-MNs penetrated the mouse skin and reached the dermis where the HF stem cells were located for sustained release of GFs. PRP-MNs based on the multifunctional tissue-engineered material GelMA/PRP show their great potential in the minimally invasive percutaneous treatment of alopecia or aesthetics.

In addition, there was growing evidence that HFs could regenerate from wounds, called wound-induced hair neogenesis (WIHN) [63–66]. β-catenin was upregulated during the wound re-epithelialization, leading to the development of embryonic HF epithelial cells [63,67]. Interestingly, here we found that the MNs group had more significant hair regrowth compared to the NC group. β-catenin expression was higher in the MNs group. Meanwhile, transcriptome analysis showed that the MNs group was upregulated in the gene sets of angiogenesis, MAPK, and PI3K signaling, suggesting that the microtrauma caused by MNs may activate local hair regrowth. AnkRD1 plays important roles in cardiac development, fibrosis, inflammation, mechanosensing, and wound healing [43]. The skin perceived stronger mechanical force from the microtrauma due to PRP-MNs intervention, and AnkRD1 acted as a gene related to mechanotransduction. In addition, the expression of TGF-β sensitive gene AnkRD1 was elevated due to the TGF-β from PRP [68]. The mechanical force could induce the formation of mild angiogenesis and skin fibrosis, suggesting that AnkRD1 might link biomechanical force to angiogenesis in skin [69]. In general, our understanding of the mechanisms behind the unique phenomenon of MNs induced hair neogenesis is expanding, and more research should involve MNs-induced WIHN to advance our understanding of MNs for hair regrowth.

The combination of GelMA/PRP matrix and detachable MNs provides a favorable microenvironment for hair development supported by comprehensive GFs and microtrauma, which is easily manufactured and stored. MNs are micron-scale needles used for drug delivery that are painless, minimally invasive, and easy to manipulate, unlike microneedling therapy (also known as percuta-

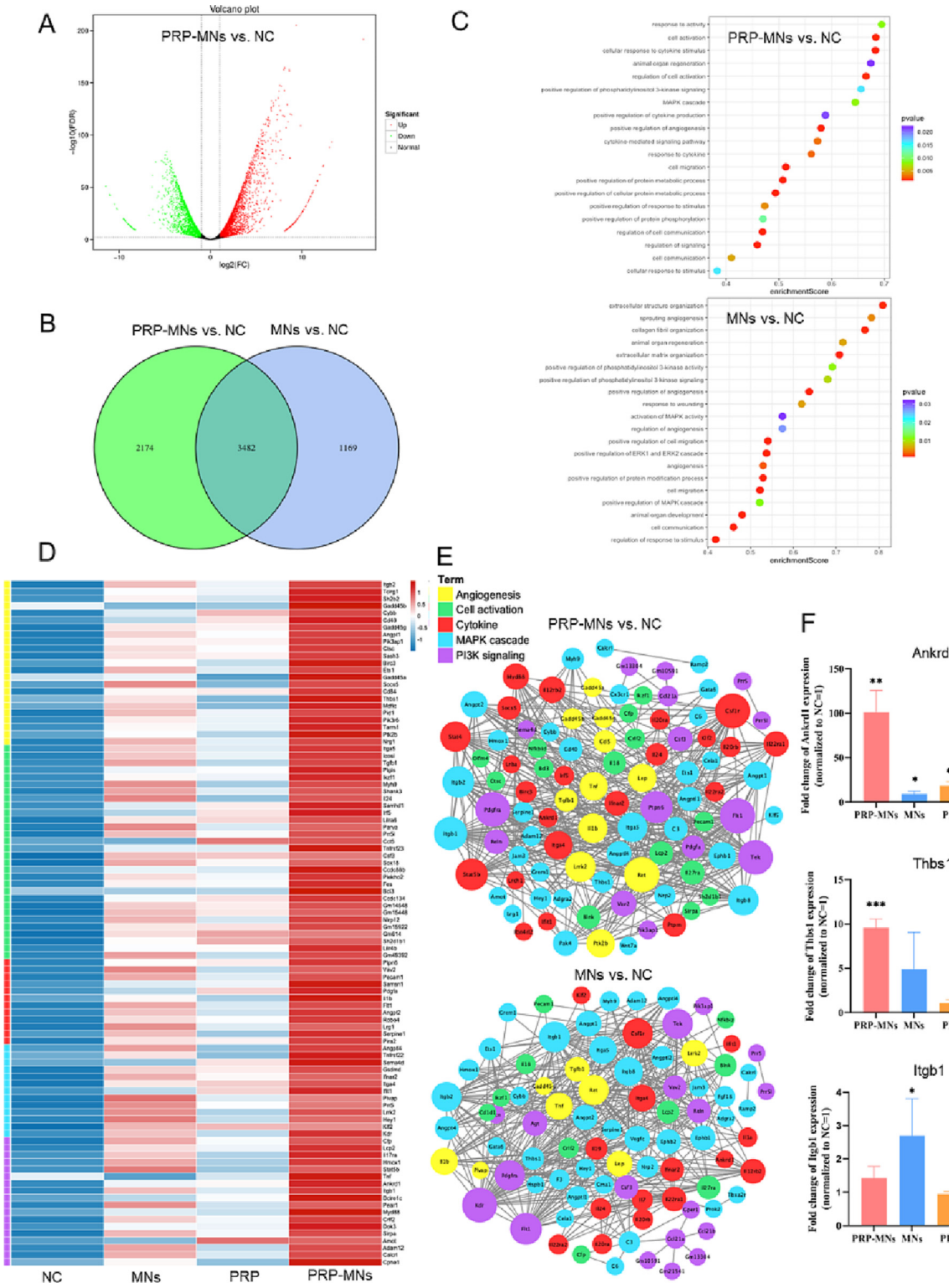

Fig. 7. Transcriptome sequencing analysis of the DEGs among PRP-MNs, MNs, PRP, and NC groups. (A) Volcano plot of DEGs (FDR < 0.01, Log(FC) > 1) comparing PRP-MNs versus NC. Red dots indicate increased expression and green indicates decreased expression after PRP-MNs application. (B) Venn diagram illustrating DEGs comparing PRP-MNs versus NC and MNs versus NC. (C) Selected upregulated 20 enrichment GO biological process terms of the GSEA analysis. The color represents the P value. (D) Heatmaps of the significantly altered genes from four groups by category. (E) Visualized PPI analysis of the DEGs. The size of a node in an interworking network is proportional to the number of edges connected to the node. (F) RT-PCR results showed the expression of Ankrd1, Thbs1, and Itgb1 after different treatments (n = 3). (For interpretation of the references to color in this figure legend, the reader is referred to the web version of this article.)

neous collagen induction), which has been reported in some clinical studies to cause pain and bleeding [70,71]. In addition to hair regrowth, PRP-MNs can benefit many other applications, such as oral and maxillofacial surgery, refractory wound, skin disease and rejuvenation, and reproductive medicine [72–74]. A recent study demonstrated that MNs could deliver to precise areas of visceral

damage with the assistance of a customized apparatus [75]. This may create new opportunities for future applications of PRP-MNs in human organs.

Conclusions

The dissolvable and detachable MN array was prepared using a double network matrix of thermal-sensitive PRP induced fibrin gel and photocrosslinked GelMA. The fibrin from PRP enhanced the mechanical ability of PRP-MNs and anchored the GFs' release in a controlled way. We verified a significant upregulation of genes related to angiogenesis, cell activation, and proliferation signaling after the application of PRP-MNs. Among them, the mechanical and TGF-β sensitive gene Ankrd1 was significantly upregulated. PRP-MNs provide a painless, minimally invasive, and sustainable effect of PRP for hair regrowth.

Experimental section

Ethics statement

This study was approved by the Ethics Committee of Nanfang Hospital (NFEC-2019–212). Volunteers provided written informed consents before participating. Animals ethical approval was obtained for all experimental procedures(NFYY-2021–0103).

Preparation and characterization of PRP

A temperature controlled PRP preparation procedure was used, which inhibited coagulation in a cryogenic environment. Basically, vein blood was collected from healthy volunteers under hypothermic conditions using precooled tubes. The PRP was obtained after a two-step centrifugation procedure (200g for 10 min at 4 °C and the next 1550g for 10 min at 4 °C). Subsequently, an appropriate amount of plasma was reserved at the bottom for resuspension of platelets and used as PRP. The a-PRP was obtained after being incubated at 37 °C for 15 mins. The lyophilization procedure were processed as described [76,77], the lyophilizing solution was added before pre-freeze PRP at −80 °C for 12 h, then freeze-dried for 24 h. FD-PRP stored at −20 °C until further use. The released supernatant was collected and stored at −80 °C. Measurement of the concentration of 3 GFs (VEGF, PDGF-BB, and TGF-β1) in PRP using ELISA kits (MultiSciences, Hangzhou). GFs in all kinds of PRP were assessed for each of the three donors. All experiments were repeated thrice.

GelMA synthesis and characterization

Briefly, GelMA was synthesized in DPBS at 50 °C via the direct reaction of gelatin with MA [78]. Once the reaction was stopped by diluting with DPBS, the reaction mixture then was dialyzed through a dialysis bag (12–14 kDa) with deionized water for 1 week to completely remove low molecular weight impurities. After lyophilization, GelMA was stored under refrigeration for further use. GelMA was characterized by FTIR spectroscopy (Bruker VERTEX 70, Germany) in the wavelength range from 4000 to 650 cm^{-1}. Synthesized GelMA and gelatin samples were dissolved in deuterium oxide (D2O) and were collected proton nuclear magnetic resonance (^{1}H NMR) spectra using a spectrometer (Bruker 400 M, Germany). The MestReNova 14.0 software was used to process the data. The integrals of the peaks were collected after correcting the reference and baseline.

Preparation of MNs patch

The MNs were fabricated using a 10 × 10 array with 800 μm tip-tip spacing PDMS micromold with 400 μm square base sides and a height of 900 μm per needle cavity. Firstly, for the preparation of the PRP-MNs patch, 1 mL of GelMA/PRP (10 wt% / 20 wt%) matrix containing 0.2 wt% lithium acylphosphinate salt (LAP) was used to fill the needle cavities and centrifuged at 4000 rpm for 10 min. This PDMS micromold was kept in the incubator (37℃) for 2–3 h to form a concentrated GelMA/PRP hydrogel and exposed to 350 mW $(cm^2)^{-1}$ UV light (405 nm). Subsequently, 1 mL of PVA solution (MW = 20,500 Da, 10 wt% in H_2O) was deposited onto the micromold and dried at an incubator overnight. The PRP-MNs patch was detached from the micromold for further use after complete desiccation. PRP was not added to the needle cavities during the preparation of the GelMA-MNs(MNs group). Additional 2.5 mg of Rhodamine B was added to make RB-MNs.

Compressive test

MNs mechanical strength was measured using a mechanical test system under dynamic forces (Instron, USA). The curves recorded the correlation between the force applied and the MNs deformation. The mechanical strength of the MNs was profiled at a constant movement speed (0.25 mm min^{-1}) of the stainless steel plate with the MNs tip placed vertically at a distance of 1.5 mm and the maximum force set to 500 N. All tests were repeated thrice.

Sem

MNs were gold plated using a sputter plating machine (Pelco, SC-7) and their surface morphology was evaluated by a field emission SEM (Hitachi S-3000 N, Japan).

Animal Experiments

8 weeks old male C57BL/6J mice were purchased from the Experimental Animal Centre at Southern Medical University (Guangzhou, China). Carefully remove the dorsum of mice with depilated cream for further PRP-MNs application. The dorsum skin along the torso was then stretched and held on the operating table to facilitate insertion of the PRP-MNs. The PRP-MNs were pressed firmly into the skin and held in place for 5 min to make the PRP-MNs absorb enough liquid. The PRP-MNs shed automatically within 2 h, leaving the PRP-MNs settled around the hair for further sustained PRP release. PRP was injected subcutaneously in the PRP group at the same dose as the corresponding PRP-MNs group. The GelMA-MNs without PRP were applied to mice as MNs group. The control group did not receive any treatment. Hair phenotype transformed was obtained over time according to the literature [39]. The percentage of hair coverage in the treated area was quantified using ImageJ software.

In vivo release study

RB-MNs were used to monitor the release of PRP-MNs. After removing the RB-MNs patch, photographs of depilated mice skin were obtained over time. In vivo fluorescence imaging of release profile were detected by an in-vivo spectrum imaging system (Spectral AMI, USA) on day0, 1, 2, 4, and 6. Use AMIView software to analyze all fluorescence intensities.

Histological and immunohistochemical analysis

Mice skins were excised and fixed in 4% paraformaldehyde overnight, and paraffin-embedded. The skins were sliced into 5 mm pieces, deparaffinized, and rehydrated before staining. Hematoxylin and eosin (Solarbio) were used to stain skin sections. For immunostaining, sections were autoclaved in antigen retrieval buffer (pH9.0 EDTA) and blocked with 10% donkey serum albumin for 30 min. The sections were probed overnight at 4 °C with the appropriate primary antibody targeting CD31 (1:1000 dilution; Abcam), β-catenin (1:200 dilution; PTG), Ki67 (1:200 dilution; Abcam), respectively. Then, Alexa Fluor 488- and 594- conjugated IgG secondary antibodies (1:400 dilution; Life Technologies) were used to incubate for another for 1 h and counterstained with DAPI (1:500 dilution; Invitrogen). The H&E-stained and immunofluorescence images were captured using a BX63 microscope (Olympus). According to the literature [39], the hair cycle of each HF was determined.

Western blot analysis

Protein isolation from mice skins used protein lysis buffer with protease inhibitors. The concentration was detected by BCA protein quantification assay. Separation of equal amounts of proteins on SDS-PAGE and transferred to the PVDF membrane. The membrane was blocked in 5% nonfat milk for 1 h and probed overnight at 4 °C with the appropriate primary antibody targeting VEGFA, β-catenin, PCNA (1:1000 dilution; PTG), and β-actin (1:8000 dilution; Cell Signaling) respectively. Then, incubated the blots with anti-rabbit IgG/HRP (1:1000 dilution; SeraCare) for 1 h and detected by a chemiluminescent substrate (BLT GelView).

RNA-sequencing analysis

RNA was collected from each group with three replicates at the same condition. NanoDrop 2000 (Thermo Scientific, USA) was served to measure RNA concentration and purity. Then, 1 μg RNA from each group was used as the input sample for sequencing. RNA-sequencing libraries were prepared using NEBNext Ultra RNA Library Prep Kit (NEB, USA) and sequenced on the Illumina platform. The clean reads were acquired by removing reads containing ploy-N and adapter. Fragments per kilobase of transcript per million mapped fragments (FPKM) were utilized to quantify gene expression. The data were accessible through Series GSE204878 in GEO database. Differential expression analysis between two groups was performed by edgeR (FDR < 0.01, Fold Change $\geq$ 2) [79]. The GSEA used GO biological process terms as the set of interest genes and controlled for p value < 0.05 and q value < 0.25 as the set of significantly enriched genes. Heatmap visualization using pheatmap (1.0.12). Protein protein interaction networks were based on the STRING database, using Cytoscape to visualize the interaction functions of genes [80].

Quantitative RT-PCR analysis

HiScript III 1st Strand cDNA Synthesis Kit (Vazyme Biotech, China) was used to reverse transcribe RNA to cDNA. Forward and reverse primers were designed respectively (Table 2). Aliquots of cDNA with ChamQ Universal SYBR qPCR Master Mix (Vazyme Biotech, China) were analyzed in triplicate by qRT-PCR experiment using CFX96 Touch Real-Time PCR Detection System (BioRAD, USA). ΔΔCT method was performed to quantify the gene expression and data was demonstrated by normalized relative fold change.

Table 2
Qrt-pcr primer sequences.

Ptpn6	**Sequence (5′->3′)**
Forward primer	CTTGGCAGGAGAACACTCGT
Reverse primer	TGCTCCCTACTGTTGGTCAC
Itgb1	**Sequence (5′->3′)**
Forward primer	CAAAGGGATGGCAGAGAAGCT
Reverse primer	CCAAAGCCAATGCGGAAGTC
Ankrd1	**Sequence (5′->3′)**
Forward primer	AACGGAAAAGCGAGAAACTGC
Reverse primer	GAAACCTCGGCACATCCACA
Thbs1	**Sequence (5′->3′)**
Forward primer	TTGGCGATGTGACAGAAAATCA
Reverse primer	TGAGCCAGTGAATCGTGGTG
β-actin	**Sequence (5′->3′)**
Forward primer	AGCAGTTGGTTGGAGCAAACATCC
Reverse primer	ACAGAAGCAATGCTGTCACCTTCC

Statistical analysis

Data were reported as mean ± SD (n = 3 or more). Student's *t* test and one-way ANOVA were used to analyze statistics (GraphPad Prism 6). Significant differences were labeled with *p < 0.05, **p < 0.01, ***p < 0.001, and ****p < 0.0001.

Compliance with Ethics Requirements

This study was approved by the Ethics Committee of Nanfang Hospital (NFEC-2019–212). Volunteers provided the written informed consents before participating. 8 weeks old male C57BL/6J mice were purchased from the Experimental Animal Centre at Southern Medical University (Guangzhou, China) and ethical approval was also obtained for all experimental procedures(NFYY-2021–0103).

CRediT authorship contribution statement

M.X., Z.H. and Y.M. supervised the project. M.X. and Y.S. conceived the conception. Y.S. designed, and conducted the experiments, with suggestions from L.Y., Y.M., M.X., and Z.H.; Y.S. performed the preparation and characterization of the PRP-MNs patches with the help of L.D., Y.Z., K.X., and Q.Q.; Y.S. performed the animal experiments and histopathologic sections with the help of J.C. and Y.H.; Y.S performed the RNA-sequencing analysis, with the help of L.Y.; Y.S. and M.X. wrote, revised, and corrected the manuscript, with the help of Z.H., Y.M., and L.Y.

Declaration of Competing Interest

The authors declare that they have no known competing financial interests or personal relationships that could have appeared to influence the work reported in this paper.

Acknowledgment

This study was funded by the National Natural Science Foundation of China(Grant No.81971889 and No.82172235) and the Natural Science Foundation of Guangdong Province (Grant No.2019A1515012170 and No.2020A1515010565). The authors would like to thank the support of Biossci Biotechnology and Shiyanjia Lab.

Appendix A. Supplementary material

Supplementary data to this article can be found online at https://doi.org/10.1016/j.jare.2023.02.014.

References

[1] Manabe M, Tsuboi R, Itami S, Osada SI, Amoh Y, Ito T, et al. Guidelines for the diagnosis and treatment of male-pattern and female-pattern hair loss, 2017 version. J Dermatol 2018;45:1031–43. doi: https://doi.org/10.1111/1346-8138.14470.

[2] Shin HS, Won CH, Lee SH, Kwon OS, Kim KH, Eun HC. Efficacy of 5% Minoxidil versus Combined 5% Minoxidil and 0.01% Tretinoin for Male Pattern Hair Loss. Am J Clin Dermatol 2007;8:285–90. doi: https://doi.org/10.2165/00128071-200708050-00003.

[3] Chen L, Zhang J, Wang L, Wang H, Chen B. The Efficacy and Safety of Finasteride Combined with Topical Minoxidil for Androgenetic Alopecia: A Systematic Review and Meta-analysis. Aesthetic Plast Surg 2020;44:962–70. doi: https://doi.org/10.1007/s00266-020-01621-5.

[4] Traish AM, Mulgaonkar A, Giordano N. The dark side of 5α-reductase inhibitors' therapy: Sexual dysfunction, high gleason grade prostate cancer and depression. Korean J Urol 2014;55:367–79. doi: https://doi.org/10.4111/kju.2014.55.6.367.

[5] Kanti V, Messenger A, Dobos G, Reygagne P, Finner A, Blumeyer A, et al. Evidence-based (S3) guideline for the treatment of androgenetic alopecia in women and in men – short version. J Eur Acad Dermatology Venereol 2018;32:11–22. doi: https://doi.org/10.1111/jdv.14624.

[6] Avram MR, Finney R, Rogers N. Hair Transplantation Controversies. Dermatol Surg 2017;43:S158–62. doi: https://doi.org/10.1097/DSS.0000000000001316.

[7] Rousso DE, Kim SW. A Review of Medical and Surgical Treatment Options for Androgenetic Alopecia. JAMA Facial Plast Surg 2014;16:444–50. doi: https://doi.org/10.1001/jamafacial.2014.316.

[8] Nadimi S. Complications with Hair Transplantation. Facial Plast Surg Clin North Am 2020;28:225–35. doi: https://doi.org/10.1016/j.fsc.2020.01.003.

[9] Lubkowska A, Dolegowska B, Banfi G. Growth factor content in PRP and their applicability in medicine. J Biol Regul Homeost Agents 2012;26.

[10] Badran KW, Sand JP. Platelet-Rich Plasma for Hair Loss: Review of Methods and Results. Facial Plast Surg Clin North Am 2018;26:469–85. doi: https://doi.org/10.1016/j.fsc.2018.06.008.

[11] Gentile P, Garcovich S. Autologous activated platelet-rich plasma (AA-PRP) and non-activated (A-PRP) in hair growth: a retrospective, blinded, randomized evaluation in androgenetic alopecia. Expert Opin Biol Ther 2020;20:327–37. doi: https://doi.org/10.1080/14712598.2020.1724951.

[12] Gentile P, Cole JP, Cole MA, Garcovich S, Bielli A, Scioli MG, et al. Evaluation of Not-Activated and Activated PRP in Hair Loss Treatment: Role of Growth Factor and Cytokine Concentrations Obtained by Different Collection Systems. Int J Mol Sci 2017;18. doi: https://doi.org/10.3390/ijms18020408.

[13] Ita K. Dissolving microneedles for transdermal drug delivery: Advances and challenges. Biomed Pharmacother 2017;93:1116–27. doi: https://doi.org/10.1016/j.biopha.2017.07.019.

[14] Pires LR, Vinayakumar KB, Turos M, Miguel V, Gaspar J. A perspective on microneedle-based drug delivery and diagnostics in paediatrics. J Pers Med 2019;9. doi: https://doi.org/10.3390/jpm9040049.

[15] Yang G, Chen Q, Wen D, Chen Z, Wang J, Chen G, et al. A Therapeutic Microneedle Patch Made from Hair-Derived Keratin for Promoting Hair Regrowth. ACS Nano 2019;13:4354–60. doi: https://doi.org/10.1021/acsnano.8b09573.

[16] Fakhraei Lahiji S, Seo SH, Kim S, Dangol M, Shim J, Li CG, et al. Transcutaneous implantation of valproic acid-encapsulated dissolving microneedles induces hair regrowth. Biomaterials 2018;167:69–79. doi: https://doi.org/10.1016/j.biomaterials.2018.03.019.

[17] Kim S, Eum J, Yang H, Jung H. Transdermal finasteride delivery via powder-carrying microneedles with a diffusion enhancer to treat androgenetic alopecia. J Control Release 2019;316:1–11. doi: https://doi.org/10.1016/j.jconrel.2019.11.002.

[18] Yuan A, Xia F, Bian Q, Wu H, Gu Y, Wang T, et al. Ceria Nanozyme-Integrated Microneedles Reshape the Perifollicular Microenvironment for Androgenetic Alopecia Treatment. ACS Nano 2021;15:13759–69. doi: https://doi.org/10.1021/acsnano.1c05272.

[19] Zhao X, Lang Q, Yildirimer L, Lin ZY, Cui W, Annabi N, et al. Photocrosslinkable Gelatin Hydrogel for Epidermal Tissue Engineering. Adv Healthc Mater 2016;5:108–18. doi: https://doi.org/10.1002/adhm.201500005.

[20] Yi R. Concise Review: Mechanisms of Quiescent Hair Follicle Stem Cell Regulation. Stem Cells 2017;35:2323–30. doi: https://doi.org/10.1002/stem.2696.

[21] Chi W, Wu E, Morgan BA. Dermal papilla cell number specifies hair size, shape and cycling and its reduction causes follicular decline. Dev 2013;140:1676–83. doi: https://doi.org/10.1242/dev.090662.

[22] Cabaro S, D'Esposito V, Gasparro R, Borriello F, Granata F, Mosca G, et al. White cell and platelet content affects the release of bioactive factors in different blood-derived scaffolds. Platelets 2018;29:463–7. doi: https://doi.org/10.1080/09537104.2017.1319046.

[23] Morris RJ, Liu Y, Marles L, Yang Z, Trempus C, Li S, et al. Capturing and profiling adult hair follicle stem cells. Nat Biotechnol 2004;22:411–7. doi: https://doi.org/10.1038/nbt950.

[24] Rezza A, Sennett R, Tanguy M, Clavel C, Rendl M. PDGF signalling in the dermis and in dermal condensates is dispensable for hair follicle induction and formation. Exp Dermatol 2015;24:468–70. doi: https://doi.org/10.1111/exd.12672.

[25] Niimori D, Kawano R, Felemban A, Niimori-Kita K, Tanaka H, Ihn H, et al. Tsukushi controls the hair cycle by regulating TGF-B1 signaling. Dev Biol 2012;372:81–7. doi: https://doi.org/10.1016/j.ydbio.2012.08.030.

[26] Yano K, Brown LF, Detmar M. Control of hair growth and follicle size by VEGF-mediated angiogenesis. J Clin Invest 2001;107:409–17. doi: https://doi.org/10.1172/JCI11317.

[27] Topkaya SN. Gelatin methacrylate (GelMA) mediated electrochemical DNA biosensor for DNA hybridization. Biosens Bioelectron 2015;64:456–61. doi: https://doi.org/10.1016/j.bios.2014.09.060.

[28] Hoch E, Schuh C, Hirth T, Tovar GEM, Borchers K. Stiff gelatin hydrogels can be photo-chemically synthesized from low viscous gelatin solutions using molecularly functionalized gelatin with a high degree of methacrylation. J Mater Sci Mater Med 2012;23:2607–17. doi: https://doi.org/10.1007/s10856-012-4731-2.

[29] Hu X, Ma L, Wang C, Gao C. Gelatin hydrogel prepared by photo-initiated polymerization and loaded with TGF-β1 for cartilage tissue engineering. Macromol Biosci 2009;9:1194–201. doi: https://doi.org/10.1002/mabi.200900275.

[30] Van Den Bulcke AI, Bogdanov B, De Rooze N, Schacht EH, Cornelissen M, Berghmans H. Structural and rheological properties of methacrylamide modified gelatin hydrogels. Biomacromolecules 2000;1:31–8.

[31] Mendes BB, Gómez-Florit M, Babo PS, Domingues RM, Reis RL, Gomes ME. Blood derivatives awaken in regenerative medicine strategies to modulate wound healing. Adv Drug Deliv Rev 2018;129:376–93. doi: https://doi.org/10.1016/j.addr.2017.12.018.

[32] Lee JW, Park JH, Prausnitz MR. Dissolving microneedles for transdermal drug delivery. Biomaterials 2008;29:2113–24. doi: https://doi.org/10.1016/j.biomaterials.2007.12.048.

[33] Yamamoto M, Ikada Y, Tabata Y. Controlled release of growth factors based on biodegradation of gelatin hydrogel. J Biomater Sci Polym Ed 2001;12:77–88. doi: https://doi.org/10.1163/156856201744461.

[34] Patel ZS, Ueda H, Yamamoto M, Tabata Y, Mikos AG. In vitro and in vivo release of vascular endothelial growth factor from gelatin microparticles and biodegradable composite scaffolds. Pharm Res 2008;25:2370–8. doi: https://doi.org/10.1007/s11095-008-9685-1.

[35] Kanematsu A, Yamamoto S, Ozeki M, Noguchi T, Kanatani I, Ogawa O, et al. Collagenous matrices as release carriers of exogenous growth factors. Biomaterials 2004;25:4513–20. doi: https://doi.org/10.1016/j.biomaterials.2003.11.035.

[36] Nichol JW, Koshy ST, Bae H, Hwang CM, Yamanlar S, Khademhosseini A. Cell-laden microengineered gelatin methacrylate hydrogels. Biomaterials 2010;31:5536–44. doi: https://doi.org/10.1016/j.biomaterials.2010.03.064.

[37] Kurita J, Miyamoto M, Ishii Y, Aoyama J, Takagi G, Naito Z, et al. Enhanced vascularization by controlled release of platelet-rich plasma impregnated in biodegradable gelatin hydrogel. Ann Thorac Surg 2011;92:837–44. doi: https://doi.org/10.1016/j.athoracsur.2011.04.084.

[38] Oh JW, Kloepper J, Langan EA, Kim Y, Yeo J, Kim MJ, et al. A guide to studying human Hair follicle cycling in vivo. J Invest Dermatol 2016;136:34–44. doi: https://doi.org/10.1038/JID.2015.354.

[39] Müller-Röver S, Handjiski B, Van Der Veen C, Eichmüller S, Foitzik K, McKay IA, et al. A comprehensive guide for the accurate classification of murine hair follicles in distinct hair cycle stages. J Invest Dermatol 2001;117:3–15. doi: https://doi.org/10.1046/j.0022-202X.2001.01377.x.

[40] Lee S-H, Yoon J, Shin SH, Zahoor M, Kim HJ, Park PJ, et al. Valproic acid induces hair regeneration in murine model and activates alkaline phosphatase activity in human dermal papilla cells. PLoS One 2012;7:e34152.

[41] Hoseong Yang S, Andl T, Grachtchouk V, Wang A, Liu J, Syu LJ, et al. Pathological responses to oncogenic Hedgehog signaling in skin are dependent on canonical Wnt/β-catenin signaling. Nat Genet 2008;40:1130–5. doi: https://doi.org/10.1038/ng.192.

[42] Magerl M, Tobin DJ, Müller-Röver S, Hagen E, Lindner G, McKay IA, et al. Patterns of proliferation and apoptosis during murine hair follicle morphogenesis. J Invest Dermatol 2001;116:947–55. doi: https://doi.org/10.1046/j.0022-202X.2001.01368.x.

[43] Murphy NP, Lubbers ER, Mohler PJ. Advancing our understanding of AnkRD1 in cardiac development and disease. Cardiovasc Res 2020;116:1402–4. doi: https://doi.org/10.1093/cvr/cvaa063.

[44] Pavlovic V, Ciric M, Jovanovic V, Stojanovic P. Platelet Rich Plasma: A short overview of certain bioactive components. Open Med 2016;11:242–7. doi: https://doi.org/10.1515/med-2016-0048.

[45] Gkini M-A, Kouskoukis A-E, Tripsianis G, Rigopoulos D, Kouskoukis K. Study of platelet-rich plasma injections in the treatment of androgenetic alopecia through an one-year period. J Cutan Aesthet Surg 2014;7:213. doi: https://doi.org/10.4103/0974-2077.150743.

[46] Lee Y, Li ZJ, Choi HI, Choi DK, Sohn KC, Im M, et al. Autologous platelet-rich plasma: A potential therapeutic tool for promoting hair growth. Dermatologic Surg 2012;38:1040–6. doi: https://doi.org/10.1111/j.1524-4725.2012.02394.x.

[47] Cervelli V, Garcovich S, Bielli A, Cervelli G, Curcio BC, Scioli MG, et al. The effect of autologous activated platelet rich plasma (AA-PRP) injection on pattern hair loss: Clinical and histomorphometric evaluation. Biomed Res Int 2014;2014:1–9. doi: https://doi.org/10.1155/2014/760709.

[48] Pietro G, Simone G, Alessandra B, Giovanna SM, Orlandi Augusto CV. The Effect of Platelet-Rich Plasma in Hair Regrowth: A Randomized Placebo-Controlled Trial. Stem Cells Transl Med 2015;4:1317–23.

[49] Gentile P. Autologous cellular method using micrografts of human adipose tissue derived follicle stem cells in androgenic alopecia. Int J Mol Sci 2019:20. doi: https://doi.org/10.3390/ijms20143446.
[50] Gentile P, Scioli MG, Bielli A, De Angelis B, De Sio C, De Fazio D, et al. Platelet-Rich Plasma and Micrografts Enriched with Autologous Human Follicle Mesenchymal Stem Cells Improve Hair Re-Growth in Androgenetic Alopecia. Biomolecular Pathway Analysis and Clinical Evaluation Biomedicines 2019;7:27. doi: https://doi.org/10.3390/biomedicines7020027.
[51] Kawase T. Platelet-rich plasma and its derivatives as promising bioactive materials for regenerative medicine: basic principles and concepts underlying recent advances. Odontology 2015;103:126–35. doi: https://doi.org/10.1007/s10266-015-0209-2.
[52] Gupta AK, Carviel JL. Meta-analysis of efficacy of platelet-rich plasma therapy for androgenetic alopecia. J Dermatolog Treat 2017;28:55–8. doi: https://doi.org/10.1080/09546634.2016.1179712.
[53] Laird ME, Lo Sicco KI, Reed ML, Brinster NK. Platelet-Rich Plasma for the Treatment of Female Pattern Hair Loss: A Patient Survey. Dermatologic Surg 2018;44:130–2. doi: https://doi.org/10.1097/DSS.0000000000001109.
[54] Mecklenburg L, Tobin DJ, Müller-Röver S, Handjiski B, Wendt G, Peters EMJ, et al. Active hair growth (anagen) is associated with angiogenesis. J Invest Dermatol 2000;114:909–16. doi: https://doi.org/10.1046/j.1523-1747.2000.00954.x.
[55] Chew EGY, Tan JHJ, Bahta AW, Ho BSY, Liu X, Lim TC, et al. Differential Expression between Human Dermal Papilla Cells from Balding and Non-Balding Scalps Reveals New Candidate Genes for Androgenetic Alopecia. J Invest Dermatol 2016;136:1559–67. doi: https://doi.org/10.1016/j.jid.2016.03.032.
[56] Amoh Y, Li L, Katsuoka K, Hoffman RM. Chemotherapy targets the hair-follicle vascular network but not the stem cells. J Invest Dermatol 2007;127:11–5. doi: https://doi.org/10.1038/sj.jid.5700486.
[57] Quan R, Du W, Zheng X, Xu S, Li Q, Ji X, et al. VEGF165 induces differentiation of hair follicle stem cells into endothelial cells and plays a role in in vivo angiogenesis. J Cell Mol Med 2017;21:1593–604. doi: https://doi.org/10.1111/jcmm.13089.
[58] Colin-Pierre C, Berthélémy N, Belloy N, Danoux L, Bardey V, Rivet R, et al. The Glypican-1/HGF/C-Met and Glypican-1/VEGF/VEGFR2 Ternary Complexes Regulate Hair Follicle Angiogenesis. Front Cell Dev Biol 2021;9:1–18. doi: https://doi.org/10.3389/fcell.2021.781172.
[59] Kanczler JM, Oreffo ROC. Osteogenesis and angiogenesis: The potential for engineering bone. Eur Cells Mater 2008;15:100–14. doi: https://doi.org/10.22203/eCM.v015a08.
[60] Gentile P, Garcovich S. Advances in Regenerative Stem Cell Therapy in Androgenic Alopecia and Hair Loss: Wnt Pathway, Growth-Factor, and Mesenchymal Stem Cell Signaling Impact Analysis on Cell Growth and Hair Follicle Development. Cells 2019;8:466. doi: https://doi.org/10.3390/cells8050466.
[61] Cheng H, Zhang J, Li J, Jia M, Wang Y, Shen H. Platelet-rich plasma stimulates angiogenesis in mice which may promote hair growth. Eur J Med Res 2017;22:1–6. doi: https://doi.org/10.1186/s40001-017-0278-5.
[62] Hojo M, Inokuchi S, Kidokoro M, Fukuyama N, Tanaka E, Tsuji C, et al. Induction of vascular endothelial growth factor by fibrin as a dermal substrate for cultured skin substitute. Plast Reconstr Surg 2003;111:1638–45. doi: https://doi.org/10.1097/01.PRS.0000053842.90564.26.
[63] Ito M, Yang Z, Andl T, Cui C, Kim N, Millar SE, et al. Wnt-dependent de novo hair follicle regeneration in adult mouse skin after wounding. Nature 2007;447:316–20. doi: https://doi.org/10.1038/nature05766.
[64] Gay D, Kwon O, Zhang Z, Spata M, Plikus MV, Holler PD, et al. Fgf9 from dermal γδ T cells induces hair follicle neogenesis after wounding. Nat Med 2013;19:916–23. doi: https://doi.org/10.1038/nm.3181.
[65] Wang G, Sweren E, Liu H, Wier E, Alphonse MP, Chen R, et al. Bacteria induce skin regeneration via IL-1β signaling. Cell Host Microbe 2021;29:777–791.e6. doi: https://doi.org/10.1016/j.chom.2021.03.003.
[66] Gentile P, Calabrese C, De Angelis B, Dionisi L, Pizzicannella J, Kothari A, et al. Impact of the Different Preparation Methods to Obtain Autologous Non-Activated Platelet-Rich Plasma (A-PRP) and Activated Platelet-Rich Plasma (AA-PRP) in Plastic Surgery: Wound Healing and Hair Regrowth Evaluation. Int J Mol Sci 2020;21:431. doi: https://doi.org/10.3390/ijms21020431.
[67] Myung PS, Takeo M, Ito M, Atit RP. Epithelial wnt ligand secretion is required for adult hair follicle growth and regeneration. J Invest Dermatol 2013;133:31–41. doi: https://doi.org/10.1038/jid.2012.230.
[68] Kanai H, Tanaka T, Aihara Y, Takeda SI, Kawabata M, Miyazono K, et al. Transforming growth factor-β/Smads signaling induces transcription of the cell type-restricted ankyrin repeat protein CARP gene through CAGA motif in vascular smooth muscle cells. Circ Res 2001;88:30–6. doi: https://doi.org/10.1161/01.RES.88.1.30.
[69] Gao Y, Zhou J, Xie Z, Wang J, Ho C kang, Zhang Y, et al. Mechanical strain promotes skin fibrosis through LRG-1 induction mediated by ELK1 and ERK signalling. Commun Biol 2019;2:1–15. https://doi.org/10.1038/s42003-019-0600-6.
[70] Zduńska K, Kołodziejczak A, Rotsztejn H. Is skin microneedling a good alternative method of various skin defects removal. Dermatol Ther 2018;31:1–8. doi: https://doi.org/10.1111/dth.12714.
[71] Ocampo-Garza SS, Fabbrocini G, Ocampo-Candiani J, Cinelli E, Villani A. Micro needling: A novel therapeutic approach for androgenetic alopecia. A Review of Literature Dermatol Ther 2020;33:1–7. doi: https://doi.org/10.1111/dth.14267.
[72] Sand JP, Nabili V, Kochhar A, Rawnsley J, Keller G. Platelet-Rich Plasma for the Aesthetic Surgeon. Facial Plast Surg 2017;33:437–43. doi: https://doi.org/10.1055/s-0037-1604240.
[73] Lynch MD, Bashir S. Applications of platelet-rich plasma in dermatology: A critical appraisal of the literature. J Dermatolog Treat 2016;27:285–9. doi: https://doi.org/10.3109/09546634.2015.1094178.
[74] Sharara FI, Lelea LL, Rahman S, Klebanoff JS, Moawad GN. A narrative review of platelet-rich plasma (PRP) in reproductive medicine. J Assist Reprod Genet 2021;38:1003–12. doi: https://doi.org/10.1007/s10815-021-02146-9.
[75] Shi H, Xue T, Yang Y, Jiang C, Huang S, Yang Q, et al. Microneedle-mediated gene delivery for the treatment of ischemic myocardial disease. Sci Adv 2020;6. doi: https://doi.org/10.1126/sciadv.aaz3621.
[76] Wolkers WF, Walker NJ, Tablin F, Crowe JH. Human platelets loaded with trehalose survive freeze-drying. Cryobiology 2001;42:79–87. doi: https://doi.org/10.1006/cryo.2001.2306.
[77] Pan L, Yong Z, Yuk KS, Hoon KY, Yuedong S, Xu J. Growth Factor Release from Lyophilized Porcine Platelet-Rich Plasma: Quantitative Analysis and Implications for Clinical Applications. Aesthetic Plast Surg 2016;40:157–63. doi: https://doi.org/10.1007/s00266-015-0580-y.
[78] Yue K, Trujillo-de Santiago G, Alvarez MM, Tamayol A, Annabi N, Khademhosseini A. Synthesis, properties, and biomedical applications of gelatin methacryloyl (GelMA) hydrogels. Biomaterials 2015;73:254–71. doi: https://doi.org/10.1016/j.biomaterials.2015.08.045.
[79] Anders S, Huber W. Differential expression analysis for sequence count data. Genome Biol 2010;11:R106. doi: https://doi.org/10.1186/gb-2010-11-10-r106.
[80] Shannon P, Markiel A, Ozier O, Baliga NS, Wang JT, Ramage D, et al. Cytoscape: A Software Environment for Integrated Models of Biomolecular Interaction Networks. Genome Res 2003;13:2498–504. doi: https://doi.org/10.1101/gr.1239303.
[81] Guo Y, Wang Y, Zhao X, Li X, Wang Q, Zhong W, et al. Snake extract–laden hemostatic bioadhesive gel cross-linked by visible light. Sci Adv 2021;7. doi: https://doi.org/10.1126/sciadv.abf9635.
[82] Xu K, Wu X, Zhang X, Xing M. Bridging wounds: tissue adhesives' essential mechanisms, synthesis and characterization, bioinspired adhesives and future perspectives. Burn Trauma 2022;10. doi: https://doi.org/10.1093/burnst/tkac033.
[83] Liu B, Wang Y, Miao Y, Zhang X, Fan Z, Singh G, et al. Hydrogen bonds autonomously powered gelatin methacrylate hydrogels with super-elasticity, self-heal and underwater self-adhesion for sutureless skin and stomach surgery and E-skin. Biomaterials 2018;171:83–96. doi: https://doi.org/10.1016/j.biomaterials.2018.04.023.